MICRO-SCALE LASER PEEN FORMING OF SINGLE CRYSTAL

Paper (M405)

Youneng Wang, Yajun Fan, Jeffrey W. Kysar, Sinisa Vukelic, Y. Lawrence Yao

Department of Mechanical Engineering
Columbia University, New York, NY 10027

Abstract

As the result of quickly increased requirement in many industrial products resulting from microtechnology, laser thermal micro-forming and micro surface treatment (microscale laser shock peening (μLSP)) have been well studied. By combining the beneficial effects of these two processes with a controlled bending deformation, microscale laser peen forming (μLPF) attracts more attention recently since it not only improves the fatigue life of the material but also shapes micro scale metallic parts at the same time. In the present study, μLSP of single crystal aluminum was presented to study anisotropic material response. Local plastic deformation was characterized by lattice rotation measured through electron backscatter diffraction (EBSD). Residual stress distributions of both sides of a peened sample, characterized by x-ray micro-diffraction, were compared with the results obtained from FEM simulation. μLPF anisotropic behavior was investigated in three effective slip systems via both the anisotropic slip line theory and numerical method. Also, the work hardening effect resulted from self-hardening and latent hardening was analyzed through comparing the results with and without considering hardening.

Introduction

It is well known that laser shock peening (LSP) can induce desirable compressive residual stresses in the target and improve its fatigue life [1, 2]. Recently, a new forming technology known as laser peen forming (LPF) which is developed from LSP has attracted more attention because of the inherent advantage of LPF. It is undesirable to form large structural components by bending or hydraulic pressing since these processes result in tensile residual stress on surfaces subject to fatigue and stress corrosion cracking. As a result, mechanical shot peen forming was developed and has been successfully used for over 40 years to shape many of these large components. Laser peen forming now can compliment this traditional forming technology and has much greater depth of residual stress, which results in 3 to 8 times greater curvature than can be achieved with mechanical shot peen forming [3]. Also, compared with shot peen forming, a desired shape may be achieved by laser peen forming with more accuracy and better repeatability, and faster.

Hackel et al. [4] employed a pulse laser beam of an energy fluence 60 to 200 J/cm^2 with a spot size ranging from 3mm×3mm to 6mm×6mm for forming shapes and contours in metal strips. They showed that the laser peen forming process can generate deep compressive stress without inducing unwanted tensile stress at the metal surface and is especially useful for thick (greater than ¾ inch thick) material that is difficult to shape or contour. Zhou et al. [5] investigated the deformation mechanisms for a special configuration; that is, a sample clamped by two concentric washers. Laser spot size they used ranges from 3 to 10mm in diameter. By using laser peen forming, metal sheet forming is realized without mold and the dimensions of the obtained shapes are determined by the boundary condition. Zhou et al. [6] further studied response of various metal sheets to LPF and presented detailed deformation characterization. The investigation showed its potential to become a flexible manufacturing process with excellent properties and short manufacturing time.

Recently, micro forming becomes a more important technology to manufacture micro metallic parts, in particular for bulk production, because of quickly increased requirement in many industrial products resulting from microtechnology [7, 8]. Laser microforming as a new technology has already been explored for a number of potential high-precision industrial applications, such as laser micro-bending of magnetic disk-drive components, adjustment of contact springs of miniature relays and reed-contacts, and accurate bending of thin plate springs, etc [9, 10]. It can be seen that most of these applications encounter cyclic loadings. Thus, it is desirable to improve fatigue life of micro-parts after microforming process.

Micro-laser peen forming (μLPF) has already attracted some attentions [11]. They showed that compressive stresses, like in the macro LPF process, can also be

induced at the surface of both sides by micro-scale laser peen forming. However, an important consideration in understanding the mechanics of μLPF at the micro-scale is that the laser spot size is likely to be in the same order of magnitude as the average grain size of the target so that the deformation is expected to occur predominately within a small number of grains. Thus in order to accurately model the process, the material properties must be treated as anisotropic and heterogeneous rather than isotropic and homogeneous. In order to gain insight into the deformation and stress fields associated with μLPF, it is advantageous to first apply the process to single crystal so that the effects of the anisotropy can first be identified in a homogeneous material.

In this paper, the effects of micro-scale laser peen forming on single crystal aluminum are studied by using both numerical and experimental methods. Beside residual stress distribution measured by x-ray micro-diffraction, peen formed crystal samples are also characterized by profilometer curvature measurement and lattice rotation of electron backscatter diffraction (EBSD). In addition, a preliminary numerical simulation based on single crystal plasticity was presented to understand the process of μLPF, especially anisotropy and effect of strain hardening. Anisotropic slip line theory was employed to compliment the numerical simulation to explain the stress and deformation state resulting from laser peen forming on a single crystal surface under plane strain conditions. Through the presented work, we can grab some main features of micro-scale peen forming and shed some shine for future work on understanding heterogeneity and associated problems of the ultra-high strain rate plastic deformation related to laser shocking.

Experiment Conditions

A frequency tripled Q-switched Nd:YAG laser ($\lambda = 355\,nm$) in TEM_{00} mode was used in micro-scale laser peen forming and the parameters of pulse duration, wavelength and beam diameter are shown in Fig. 1. If a line loading is applied parallel to a <110> direction in a FCC crystal, certain slip systems act cooperatively which enable approximate plane strain deformation conditions to be achieved [12]. Therefore, a line of μLSP shocks parallel to a <110> direction was created on the sample surface with a 25μm spacing because this spacing results in approximate 2-D deformation. Pulse energies, 202 and 280μJ, corresponding to laser intensities of 3.57 and 4.95GW/cm^2, respectively, were applied. A thin layer of high vacuum grease (about 10 microns thick) was spread evenly on the sample surface to isolate the thermal effect from the coating, and a 16μm thick polycrystalline aluminium foil, chosen for its relatively low threshold of vaporization, was tightly pressed onto the grease. The sample was placed in a shallow container filled with distilled water around 1 mm above the sample's top surface to confine the produced plasma. The induced deformation is due to shock pressure and not due to thermal effects since only the coating is vaporized during the process [2].

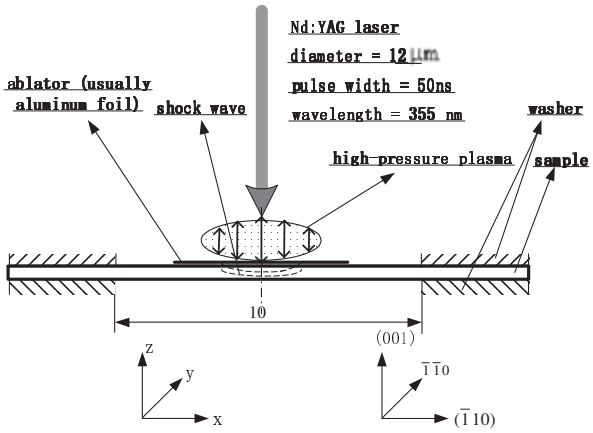

Fig. 1 Sample geometry and laser peen forming condition

In order to investigate the effects of specimen thickness under the same laser energy, the samples of single crystal aluminium with 150μm, 200μm and 300μm thickness have been chosen, which have normal orientation of (001) as shown in Fig. 1. The samples were cut to the dimension of 20mm×3mm by using wire electrical discharge machining (EDM) and mounted to holders as shown in Fig.1 carefully to make them as flat as possible. The sample surface on both sides was polished mechanically first, in order to remove the thermal affected layer by EDM, and then electro-polished to eliminate residual stress. Before shocking process, the pre-bending is measured by using a Mitutoyo SJ-201P profilometer as shown in Fig. 2 and the samples with a pre-bending less than 8μm were chosen to minimize the pre-bending effects.

Post Peen Forming Material Characterization

After laser peen forming, the sample was characterized by curvature change, residual stress distribution and lattice rotation. The first characterization is necessary for studying capability of micro-scale curvature adjustment by μLPF and second for its potential to improve fatigue life. Lattice rotation, accounting for the rotation part in the polar decomposition of elastic deformation, is induced by plasticity and can be quantitative analyzed by electron backscatter

diffraction (EBSD). Thus, we can directly compare the experimental results of lattice rotation with simulation results.

The curvature change is characterized by using profilometer measurement, whose range in depth direction is 350μm with the resolution 0.4μm. The measuring force is 4mN, which assures the detector has no bending effect on the samples while measuring. Residual stresses were estimated from x-ray micro-diffraction profiles, which were collected from Beamline X20A (synchrotron radiation sources) at National Synchrotron Light Source at Brookhaven National Lab. X-ray of X20A can be focused by a tapered glass capillary to spot sizes as small as 3 microns. Complete details of x-ray micro-diffraction experiment and the corresponding evaluation method of sub-profile analysis can be found in Chen, et al.[13] For lattice rotation, the crystallographic orientation of peened area for both top and bottom surfaces was collected using EBSD, which provided information about the lattice rotation on the shocked area. EBSD data was collected using a system supplied by HKL Technology and attached to a JEOL JSM 5600LV scanning electron microscope.

FEM Simulation Conditions

In order to further understand μLPF process, the numerical simulation of micro-scale peen forming on the single crystal aluminum was carried out by using quasi-static loading. The numerical simulation will allow more precise understanding of anisotropy effects associated with μLPF. In addition, the lattice rotation is calculated numerically and residual stress can be estimated. Subsequent simulations which account for more realistic material constitutive behavior, as well as accounting for inertial contributions, will concentrate on how the additional effects modify the baseline solution. Thus, it is expected that these simulations will lay the ground work for more realistic simulations.

Finite element simulations based on single crystal plasticity [14] were carried out with a user-material subroutine (UMAT), which was written by Huang[15] and modified by Kysar [16]. It is incorporated into the finite element analysis using the general purpose finite element program ABAQUS/Standard. In the UMAT, the {111}<110> slip systems in FCC metal are employed and a critical resolved shear strength $\tau_{CRSS} \approx 1MPa$ is assumed for each of the slip systems. The element used in the simulation was a plane strain reduced integration, hybrid element (CPE4RH) and total simulation size is 384μm×192μm (thickness×width). The mesh size is about 0.1μm in the area close to the loading and 1.5μm far away from the loading. As for boundary conditions of the plane strain model, the applied surface tractions correspond to the applied pressure on the shocked surface. At the bottom surface, the vertical displacement is specified to be zero and the outer edges are traction free. In the simulation, elastic-ideally plastic behavior is assumed. The simulation ignores rate and inertial effects. The loading on the surface has a Gaussian distribution: $P(x) = P_0 \exp\left(-\frac{x^2}{2R^2}\right)$, where x is the radial distance from the center of the laser beam and R is the radius of plasma. Following Zhang and Yao [17], the resulting plasma radius is $R = 9.5\mu m$ at the end of the laser pulse for the laser beam diameter 12μm. The plasma is expected to expand further after 50ns, but the resulting pressure decreases very quickly so that effect is ignored [2, 17]. The simulation is divided into two steps, loading and relaxation step, and the maximum magnitude of applied pressure is determined by trial and error method. The pressure magnitude was varied until the simulation result of curvature change matched experimental findings. Rate dependence used is a power-law relationship proposed by Hutchinson [18] and described by Connolly and McHugh [19], Huang [15], Kysar [20], Peirce et al. [21], and Savage et al. [22]:

$$\dot{\gamma}_k = \dot{\gamma}_0 \operatorname{sgn}\tau_k \left\{\left|\frac{\tau_k}{g_k}\right|\right\}^m \qquad (1)$$

where is $\dot{\gamma}_0$ the reference strain rate, τ_k is the applied resolved shear stress, m is the rate sensitivity exponent, and g_k is related to critical resolved shear stress of the kth-slip system, as given by Peirce et al.[21] In this simulation, $\dot{\gamma}_0 = 10^{-3}$ and $m = 50$.

FEM Simulation with Work Hardening

In LPF, the target is subjected to very strong shock pressures (>1 GPa), the interaction time is very short (<100 ns), and the strain rate is very high (>100,000 s^{-1}). A review of the constitutive equations for such high strain rates was given by Meyer [23]. The simplest model to describe the work hardening behavior of metals is Ludwik equation: $Y = A + B\varepsilon^n$ at ambient temperature and quasistatic loading, where Y is the yield strength, n, A and B are material constants, and ε is the equivalent plastic strain. For single crystals of face-centered-cubic (FCC) metals, work hardening experiences three stages [24]. During stage I, dislocations move on a single set of parallel slip planes and there is little work hardening. Stage II hardening

starts when intersecting slip systems are activated and dislocations moving on the intersecting glide planes entangle each other. Dislocation density increases rapidly with increasing strain in stage II. At higher strains, stage III happens when the rate of work hardening diminishes with increasing strain because screw dislocations can cross-slip from one slip plane to another and so by-pass obstacles and annihilate dislocations of opposite sign in neighboring planes at sufficiently high stresses. For most polycrystalline cubic metals, stage III work hardening is the dominant mode observed in tests on most at room temperature. Because approximately linear stage II hardening may be present in the early stages of straining, Ludwik equation is often poor at low strains for FCC single crystals of metals.

In this paper, Asaro's hardening theory of single crystal [14] has been applied, in which the critical shear stress τ_0^k of the Schmid law is determined by the current dislocation density and substructure, and represents variation of hardness of material due to work hardening. Since work hardening of slip system depends on shear deformation of slip systems, variation of τ_0^k may be estimated by

$$\Delta\tau_0^k = h_1^k|\Delta\gamma_1| + h_2^k|\Delta\gamma_2| + h_3^k|\Delta\gamma_3| + h_4^k|\Delta\gamma_4| + \cdots = \sum_i h_i^k|\Delta\gamma_i| \quad (2)$$

where h_i^k expresses hardening rate against increment of shear deformation $\Delta\gamma_i$ on each slip system. When k equals to i, h_i^k represents hardening by glide on its own slip system. When k is not the same as i, h_i^k represents hardening by glide on other slip systems. The former is called the self hardening, and the latter is called the latent hardening. It is found that latent hardening rate does not depend on combination of slip systems. The ratio denoted by q between latent hardening rate and self hardening rate can be evaluated by the following equation [14]:

$$h_i^k = qh + (1-q)h\delta_{ij} = h\begin{bmatrix} 1 & q & q & \cdots & q \\ q & 1 & q & \cdots & q \\ q & q & 1 & & \vdots \\ \vdots & \vdots & & \ddots & q \\ q & q & \cdots & q & 1 \end{bmatrix} \quad (3)$$

and q=1.4 is best to match simulation with experimental results. Where h is given by

$$h = h_0 \operatorname{sech}^2\left(\frac{h_0\gamma}{\tau_{\max}^k - \tau_0^k}\right)$$

$$\gamma = \sum_i |\Delta\gamma_i|$$

where $\tau_{\max}^k$ is the maximum value of yield shear stress, τ_0^k is the initial value of yield shear stress, and h_0 is a material constant. In this paper, $h_0 = 8.9\tau_0$ and $\tau_{\max}^k = 1.8\tau_0$ are used [14].

Results and Discussion

Curvature Changes

Our previous work [11] showed that 100μm poly copper with 3.57GW/cm^2 laser intensity was bent downward while the same sample was bent upward with high energy of 4.95GW/cm^2 intensity. In this paper, in order to verify deformation mechanism of LPF, these two levels of laser energy were used for single crystal aluminium as well, but the minimum thickness of 150μm was selected instead of 100μm because single crystal aluminium is much softer than poly copper sample. For the aluminium single crystal, as it can be seen in Figs. 3 and 4, 150μm thick sample was bent downward with low laser energy of 3.57GW/cm^2 intensity and bent upward with 4.95GW/cm^2 intensity. This trend is consistent with the case of poly copper samples and detailed explanation can be found in our previous work [11]. In order to examine thickness effects, we have also applied laser shocks of the same intensity (3.57GW/cm^2) onto specimens with different thickness. Fig. 2 shows the curvature change of 200μm and 300μm thick samples and it can be seen that the curvature change become smaller as thickness increases. For the 200μm sample, it was bent downward 11μm and the corresponding bending angle is about 0.13°.

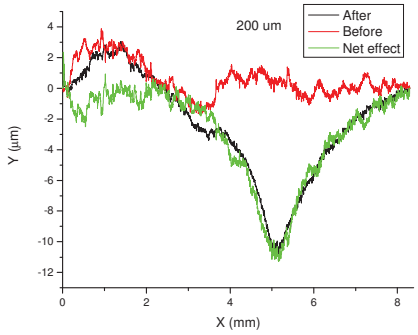

Fig. 2 Curvature measurement on the bottom side before and after peen forming for 200μm sample with 3.57GW/cm^2 laser intensity

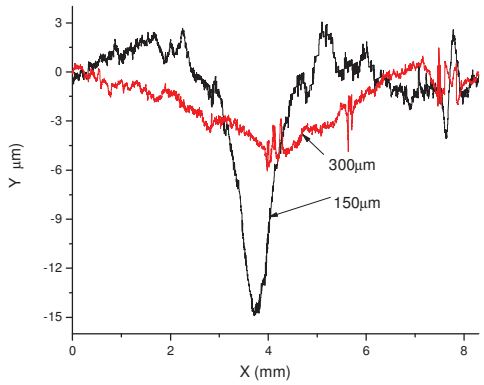

FIG. 3 Curvature measurement for 150um and 300um sample with low energy

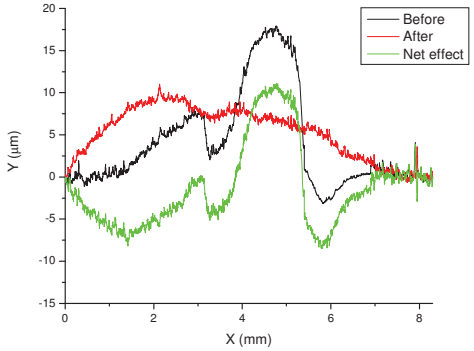

Fig. 4 Curvature measurement for 150um with high energy

Residual Stress Distribution

In order to spatially resolve the residual stress induced by μLPF, measurements were made on both top and bottom surfaces along the lines perpendicular to the peened line. The spacing between adjacent measurement points is 10μm and the corresponding x-ray diffraction profile at each position is recorded and repeated for each scan line. Fig. 5 shows the residual stress distribution for 200μm sample with laser energy of 3.57GW/cm^2. It can be seen that a compressive residual stress is generated near the center of peened region on the bottom side and there is a tensile residual stress near the center bordered by a region of compressive stress on the top side. Although the laser spot size is only 12μm, the high shock pressure in μLPF can generate significant compressive residual stresses over a much larger region, up to 200μm. For 150μm samples with two laser energy levels, residual stress distributions are shown in Fig. 6. Measurements indicate that high laser energy of 4.95GW/cm^2 intensity induces compressive residual stress in both sides and the pattern with low energy of 3.57GW/cm^2 is the same as the one of 200μm. Similar to the results of previous work [11], the pattern of residual stress corresponds to the bending mechanism; that is, for bending upward, residual stresses are compressive on both sides and tensile on the top and compressive on the bottom for bending downward.

Fig. 7 shows the simulation results of residual stress contour for 200μm sample with 3.57GW/cm^2 laser intensity. Residual stress patterns for the case when we observe downward bending are in good agreement with the experimental results for different thickness. However, for upward bending case of 150μm thick specimen under laser intensity 4.95GW/cm^2, the simulation model is limited to grab the corresponding curvature change because of quasi-static loading.

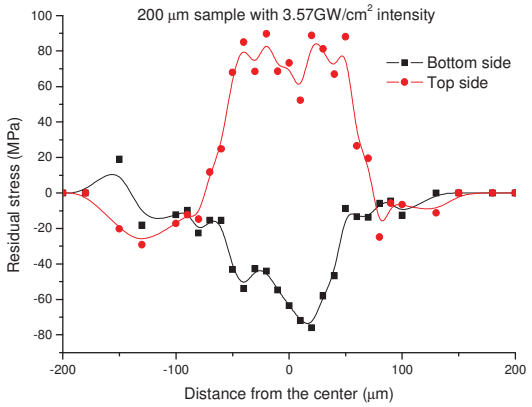

Fig. 5 Residual stress distribution by X-ray micro-diffraction for 200μm sample

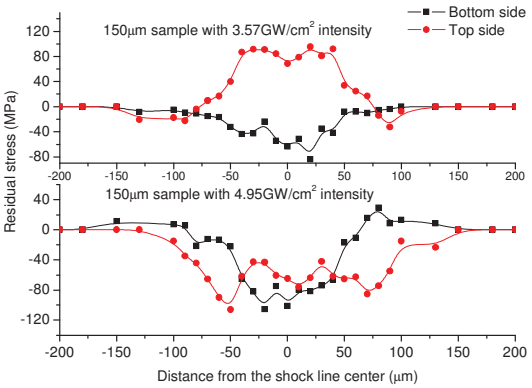

Fig. 6 Residual stress distribution by X-ray micro-diffraction for 150μm with two laser energy levels

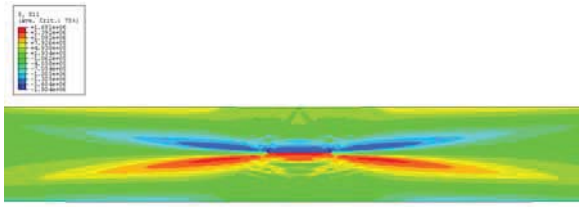

Fig. 7 Residual stress contour by FEM simulation

Lattice Rotation Field by EBSD

All EBSD data were acquired in the automatic mode, using external beam scanning and employing a 3µm step size. The scan area is about 350µm×150µm on the shocked region as shown in Figs. 8(a) and (b), respectively. The EBSD results from each individual scan comprise data containing the position coordinates and the three Euler angles which describe the orientation of the particular interaction volume relative to the orientation of the specimen in the SEM, allowing the in-plane and the out-of-plane lattice rotations to be calculated relative to the known undeformed crystallographic orientation, which serves as the reference state.

The lattice rotation contour map of bottom surface is shown in Fig. 4 (a) for 200µm sample. Fig. 4(b) shows the lattice rotation contour map for the top side. The red region corresponds to counter-clockwise rotation about the y-axis (as defined in Fig. 1) which is positive and the blue region corresponds to clockwise rotation which is negative. Similar to µLSP process, the lattice rotation on top surface caused by µLPF is zero (green region) far away from the shocked line which corresponds to the shock-free region. The lattice rotation distribution along the shocked line is quite uniform which suggests the approximate two-dimensional deformation state mentioned before. The lattice rotation value is up to ±3° between ±120µm from the center of shocked line on the top surface and the rotation direction is anti-symmetric about the shock line on both sides. The rotation contour of bottom side approximately corresponds to the bending curvature since lattice rotation in each side of shock line is almost constant and rotation value is close to the bending angle. The difference is because that the bending angle measured by Profilometer reflects overall curvature while lattice rotation represents the bending angle close to shock line.

Fig. 9 presents the lattice rotation contours for 150µm and 300µm samples' top surface with low energy of 3.57GW/cm^2. They showed similar patterns as that of 200µm sample, but the maximum angle of lattice rotation is different and corresponds to the thickness. Maximum rotation angle decreases as the thickness increases, for example, 3.5° for 150µm, 3° for 200µm and 2° for 300µm sample, because of harder bending when the thickness increases. Lattice rotation by simulation for 200µm is shown in Fig. 10, which shows the same contour for both sides and is corresponding to the experimental of bottom side. But for the top surface feature of lattice rotation, it is impossible to be grabbed by simulation with quasi-static loading. Therefore, it is necessary to carry out simulation under dynamic loading condition in future.

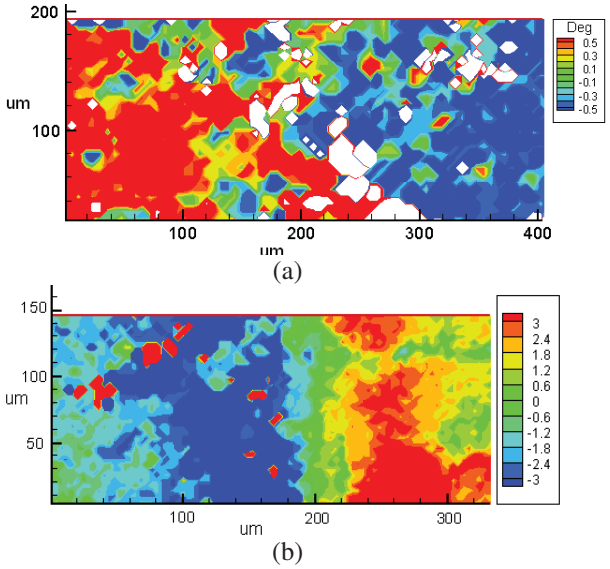

Fig. 8 Lattice rotation distribution by EBSD measurement for 200µm sample with 3.57GW/cm^2 laser intensity: a) bottom side; b) top side

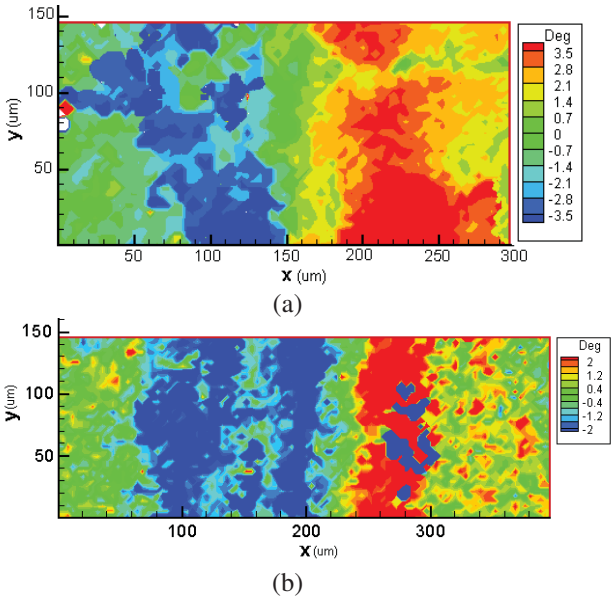

Fig. 9 Lattice rotation by EBSD for 150um and 300um sample top side with low energy: a) 150um; b) 300um

Fig. 10 Lattice rotation contour by FEM simulation for 200μm sample

Shear Strain Distribution in Each Slip System

Fig.11 shows the shear strain distribution for the three slip systems as well as the total shear strain by FEM simulation without considering work-hardening; that is, Fig. 11(a) shows the distribution of slip system *i* and the distribution of slip system *iii* is symmetric with that of slip system *i* and shear strain is almost zero for slip system *ii* so that it is not included in Fig.11. It can be seen that plastic deformation is caused mainly by slip system *i* and *iii* because Schmid's factor is zero for slip system *ii*. It is of great interest to understand the logics behind these shear distributional pattern for each slip system. In this paper, anisotropic slip line theory is applied to preliminary explain these distributions.

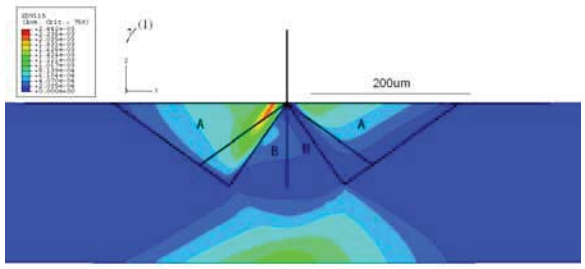

(a)

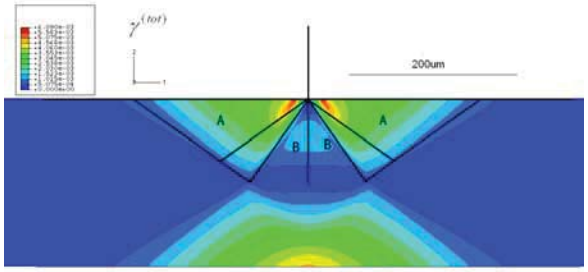

(b)

Fig. 11 Shear strain contour in slip system: a) slip system *i*; b) total shear strain

Construction of slip field According to the anisotropic slip line theory [12, 20, 29] when loading is applied along (110) direction in FCC crystals three out of twelve slip systems will be activated. Rice [29] employed anisotropic slip line theory to solve punch problem. Wang et al. extended this work to the μLSP, where laser induced Gaussian pressure loading is approximated as punch with non-uniform pressure distribution. Furthermore in μLSP domain of interest is considered to be semi-infinite and deformation is local. On the other hand in μLPF case nature of deformation mechanism is different and global deformation has to be taken into account. Width of Gaussian pressure loading is order of magnitude smaller than width of specimen, thus from global point of view it can be assumed to be point load that causes bending. Therefore following [12, 29], center of the Gaussian pressure loading can be seen as the point of singularity in which centered fan is placed. Slip line field constructed in such way is depicted in Fig. 12. Comparison of proposed explanation shows good agreement with numerical simulation, as shown in Fig. 11(b) for the total shear strain distribution. It also agrees well with the numerical solution of shear strain distribution for slip system *i*. However, this issue requires further attention, more detailed analytical study of stress field based on the anisotropic slip line theory is required, which would lead to closed form solution of this problem.

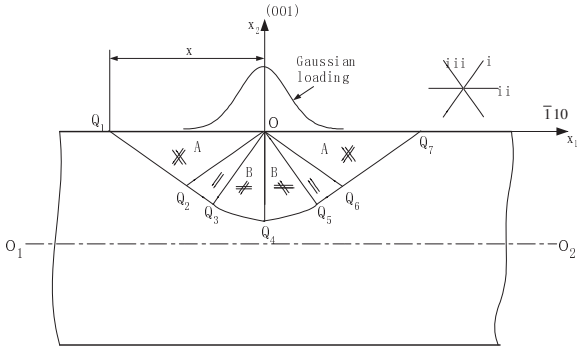

Fig. 12 Geometry of slip line field for a Guassian distribution of peen forming

Effect of Work Hardening

In order to lay some ground for future realistic numerical simulation, which account for the material behavior under high dynamic loading with extreme high strain rate (10^7~10^9 s^{-1}) including both work hardening and strain rate effects on LPF, here we only consider the effects of work hardening first to simplify the problem.

As expected, the target is hard to be deformed when encountering effects of work hardening. Fig. 13 shows the difference of the bending curvature for the single crystal aluminium sample with and without considering work hardening for the same simulation condition. The maximum displacement with work hardening consideration is around 7μm and without work hardening is about 10μm. For work hardening effects on total shear strain corresponding to Fig. 11(b), it is found that work hardening almost has no effect on the plastic deformation width under the previously defined simulation conditions, but the maximum of total shear strain on the top surface is reduced almost 40% if work hardening is considered, as shown in Fig. 14. In addition, it is of great interest to look into shear strain distribution in each slip system with work hardening effects because anisotropic character associated with micro-scale laser peen forming is observed in FEM simulation results under quasi-static loading without considering work hardening and high strain rate effects. Comparing simulation results of shear strain distribution in each slip system without and with work hardening, it is found that the patterns and effected area is same for these two conditions. Therefore, we have more confidence that this anisotropy is more likely associated with μLPF, but the magnitude of shear strain will become smaller if considering high strain rate effects.

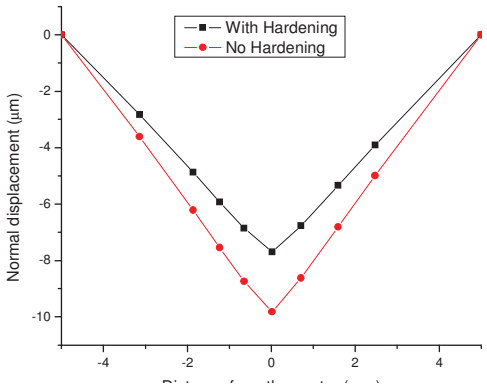

Fig. 13 Normal displacement of FEM simulation with and without work hardening

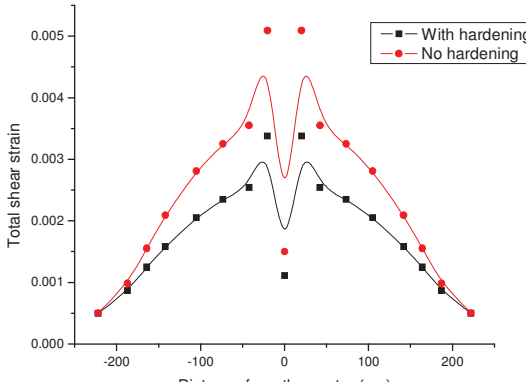

Fig. 14 Total shear strain contour of FEM simulation with work hardening

Conclusions

In this paper, μLPF of single crystal aluminum with orientation [001] under approximate plane strain condition was investigated using both, experimental and numerical methods.Construction of the slip line field is proposed. Like μLSP, it was found that the potential exists for rapid changes in field variables for μLPF as well. The lattice rotation field under laser peen forming is found to be anti-symmetric on both top and bottom surfaces and top side is similar as that of μLSP, but bottom side is proximately accounting for the curvature slope of global deformation. The magnitude of lattice rotation on the top surface increases when sample thickness becomes thinner, such as ±2° for 300μm, ±3° for 200μm and ±3.5° for 150μm, and lattice rotation covers a region around ±150μm across the shock line. Compared with previous work of μLPF on the polycrystalline copper, it was found that anisotropy has little effect on bending mechanisms. Similarly, residual stresses are compressive on bottom side for both upward and downward bending of single crystals, and are tensile on top side for bending downward and compressive for bending upward. The methodologies and results presented herein enable a systematic study of the micro scale laser peen forming process and shed some light on understanding laser peen forming process under micro scale length.

Acknowledgement

This work is supported by the National Science Foundation under grants DMI-02-00334 and DMI-06-20741. JWK would like acknowledge support by the National Science Foundation under the Faculty Early Career Development (CAREER) Program with grant

CMS-0134226. Single crystal sample preparation provided by Dr. Yongxue Gang is also acknowledged.

References

[1] Clauer, A.H. and Holbrook, J.H. (1981) Shock Waves and High Strain Phenomena in Metals-Concepts and Applications, New York, Plenum, p. 675.

[2] Zhang, W. and Yao, Y.L. (2000) Micro scale laser shock processing of metallic components, ASME Journal of Manufacturing Science and Engineering 124, pp.369-378.

[3] Hackel, L.A. (2003) Laser peening and laser peenforming: new tools for inducing surface stress, Light Metal Age, December.

[4] Hackel, L.A. and Harris, F. B. (2002), Contour forming of metals by laser peening, US Patent 6410884.

[5] Zhou, M., Zhang, Y., and Cai, L. (2002) Laser Shock Forming on Coated Metal Sheets Characterized by Ultrahigh-Strain-Rate Plastic Deformation, Journal of Applied Physics 91, pp. 5501-5503.

[6] Zhou, M., Zhang, Y.K., and Cai, L. (2003) Ultrahigh-Strain-Rate Plastic Deformation of a Stainless-Steel Sheet with TiN Coatings Driven by Laser Shock Waves, Applied Physics A-Materials Science & Processing **77**, pp. 549-554.

[7] Geiger, M., Kleiner, M., Eckstein, R., Tiesler, N., and Engel, U. (2001) Microforming, CIRP Ann. 50, pp.445-462.

[8] Cao, J., Krishnan, N., Wang, Z., Lu, H., Liu, W.K., and Swanson, A. (2004) Microforming: Experimental Investigation of the Extrusion Process for Micropins and its Numerical Simulation Using RKEM, ASME Journal of Manufacturing Science and Engineering 126, pp. 642-652.

[9] Otsu, M., Wada, T., and Osakada, K. (2001) Micro-bending of thin spring by laser forming and spark forming, CIRP Annals - Manufacturing Technology 50, pp.141-144.

[10] Esser, G., Schemidt, M., and Dirscherl, M. (2003) Laser Adjustable Actuators for High-Accuracy Positioning of Micro Components, Proceedings of SPIE - The International Society for Optical Engineering, Fourth International Symposium on Laser Precision Microfabrication 5063, pp.177-182.

[11] Wang, Y., Fan, Y., Vukelic, S., and Yao, Y.L., (2007) Energy Level Effects on Deformation Mechanism in Micro-scale Laser Peen Forming", SME J. of Manufacturing Process, accepted.

[12] Rice, J.R., (1987) Tensile Crack Tip Fields in Elastic-ideally Plastic Crystals, Mechanics of Materials 6, pp.317-335.

[13] Chen, H., Yao, Y.L., and Kysar, J.W. (2004) Spatially Resolved Characterization of Residual Stress Induced by Micro Scale Laser Shock Peening, ASME Journal of Manufacturing Science and Engineering 126, pp. 226-236.

[14] Asaro, R.J. (1983) Micromechanics of Crystals and Polycrystals, Adv. Appl. Mech. 23, pp.1-115.

[15] Huang, Y. (1991) A User-Material Subroutine Incorporating Single Crystal Plasticity In the ABAQUS Finite Element Program, Mech Report 178, Division of Applied Sciences, Harvard University, Cambridge, MA.

[16] Kysar, J.W. (1997) Addendum to "A User-Material Subroutine Incorporating Single Crystal Plasticity In the ABAQUS Finite Element Program, Mech Report 178", Division of Engineering and Applied Sciences, Harvard University, Cambridge, MA.

[17] Zhang W., and Yao Y.L. (2001) Micro-scale Laser Shock Processing: Modeling, Testing, and Microstructure Characterization, SME J. of Manufacturing Processes 3, pp. 128-143.

[18] Hutchinson, J.W. (1968) Singular behavior at the end of a tensile crack tip in a hardening material, Journal of the Mechanics and Physics of Solids 16, pp.13–31.

[19] Connolly P. and McHugh P. (1999) Fracture modelling of WC–Co hard metals using crystal plasticity theory and the Gurson model, Fatigue Fract. Eng. Mater. Struct. 22, pp.77–86.

[20] Kysar, J.W. (2001) Continuum simulations of directional dependence of crack growth along a copper/sapphire bicrystal interface: part I, experiments and crystal plasticity background, J. Mech. Phys. Solids 49, pp.1099–1128.

[21] Peirce, D., Asaro, R., and Needleman, A. (1983) Material rate dependence and localised deformation in crystalline solids, Acta Metall. Mater. 31, pp.1951–1976.

[22] Savage, P., Donnell, B.P.O., McHugh, P.E., Murphy, B., and Quinn, D. (2004) Coronary stent strut size dependent stress–strain response investigated using micromechanical finite element models, Ann. Biomed. Eng. 32, pp.202–211.

[23] Meyer, L.W. (1992), Shock-wave and High-Strain-Rate Phenomena in Metals, New York, Marcel Dekker, Inc., pp. 49-68.

[24] Wilson, D.V. (1974) Relationships between microstructure and behaviour in the uniaxial tensile test, Journal of Physics D: Applied Physics 7, pp. 954-968.

[25] Kysar, J.W. and Briant, C.L. (2002) Crack Tip Deformation Fields in Ductile Single Crystals, Acta Materialia 50, pp.2367-2380.

[26] Hencky, H. (1923) Über einige statisch bestimmte Fälle des Gleichgewichts in plastischen Körpern and, Z. angew. Math. Mech. 3, pp.241–251.

[27] Hill, R. (1950) The Mathematical Theory of Plasticity, Clarendon Press, Oxford.

[28] Booker, J.R. and Davis, E.H., A General Treatment of Plastic Anisotropy under Conditions of Plane Strain, Journal of the Mechanics and Physics of Solids 20, pp.239-250.

[29] Rice, J.R. (1973) Plane strain slip line theory for anisotropic rigic/plastic materials, Journal of the Mechanics and Physics of Solids 21, pp.63-74.

Meet the authors

Youneng Wang is an engineer in Michelin North America. He received his Ph.D. from Columbia University in 2006. His research interests are laser micro-manufacturing.

Yajun Fan is an engineer in Caterpillar. He received his Ph.D. from Columbia University in 2006. His research interests are laser shock peening and laser micromachining.

Jeffrey W. Kysar is an Associate professor at Columbia University. He received his Ph.D. from Harvard University and his research interests are micromechanics of facture in ductile materials, and multi-scale experiments and modeling of fracture.

Sinisa Vukelic is a Ph.D candidate at Columbia University. He received his BS from University of Belgrade. His research interests are laser shock peening and laser micromachining.

Y. Lawrence Yao is a Professor at Columbia University. He received his Ph.D. from the University of Wisconsin-Madison in 1988. He is interested in multidisciplinary research in manufacturing and design, nontraditional manufacturing processes and laser materials processing. He serves on the Board of Directors of LIA.